

Thomas Allkemper, MD
 Bernd Tombach, MD
 Wolfram Schwandt, MD
 Harald Kugel, PhD
 Matthias Schilling, MD
 Otfried Debus, MD
 F. Möllmann, MD
 Walter Heindel, MD

Index terms:

Brain, hemorrhage, 13.367, 13.433, 13.434
 Brain, MR, 13.121412, 13.121413, 13.121415, 13.121416, 13.12146
 Magnetic resonance (MR), high-field-strength imaging, 13.121412, 13.121413, 13.121415, 13.121416, 13.12146

Published online before print
 10.1148/radiol.2323030322
 Radiology 2004; 232:874–881

Abbreviations:

CNR = contrast-to-noise ratio
 FLAIR = fluid-attenuated inversion recovery
 ICH = intracerebral hemorrhage
 SI = signal intensity

¹ From the Departments of Clinical Radiology (T.A., B.T., W.S., H.K., W.H.), Neurology (M.S.), Pediatrics (O.D.), and Neurosurgery (F.M.), University of Muenster, Albert-Schweitzer-Strasse 33, 48149 Muenster, Germany. Received March 1, 2003; revision requested May 23; final revision received January 19, 2004; accepted February 13. Address correspondence to T.A. (e-mail: allkemp@uni-muenster.de).

Authors stated no financial relationship to disclose.

Author contributions:

Guarantors of integrity of entire study, T.A., B.T., W.H.; study concepts and design, T.A., B.T., W.H., H.K.; literature research, T.A., B.T.; clinical studies, T.A., W.S., B.T.; data acquisition, T.A., M.S., O.D., F.M., H.K.; data analysis/interpretation, T.A., B.T., W.S., H.K., W.H.; statistical analysis, H.K., T.A.; manuscript preparation, T.A., B.T., W.S., H.K.; manuscript definition of intellectual content, T.A., B.T., W.S., M.S., O.D., F.M., W.H.; manuscript editing, T.A., B.T., W.S., H.K.; manuscript revision/review, T.A., B.T., W.H.; manuscript final version approval, all authors

© RSNA, 2004

Acute and Subacute Intracerebral Hemorrhages: Comparison of MR Imaging at 1.5 and 3.0 T—Initial Experience¹

PURPOSE: To assess and describe the appearance of intracerebral hemorrhage (ICH) at 3.0-T magnetic resonance (MR) imaging as compared with the appearance of this lesion type at 1.5-T MR imaging.

MATERIALS AND METHODS: Sixteen patients with 21 parenchymal ICHs were examined. ICHs were classified as hyperacute, acute, early subacute, late subacute, or chronic. Patients underwent 1.5- and 3.0-T MR imaging with T2-weighted fast spin-echo, fluid-attenuated inversion-recovery (FLAIR), and T1-weighted spin-echo (1.5-T) and gradient-echo (3.0-T) sequences within 4 hours of each other. The central (ie, core) and peripheral (ie, body) parts of the ICHs were analyzed quantitatively by using contrast-to-noise ratio (CNR) calculations derived from signal intensity (SI) measurements; these values were statistically evaluated by using the Mann-Whitney *U* test. Two readers qualitatively determined SIs of the cores and bodies of the ICHs, degrees of apparent susceptibility artifacts, and lesion ages. The χ^2 test was used to determine statistically significant differences.

RESULTS: With the exception of the bodies of late subacute ICHs at 3.0-T T2-weighted imaging, which had increased positive CNRs and SI scores ($P \leq .05$), all parts of the ICHs at all stages showed increased negative CNRs and SI scores at 3.0-T FLAIR and T2-weighted imaging, as compared with these values at 1.5 T ($P \leq .05$). No significant CNR or SI score differences at any ICH stage were observed between 1.5-T spin-echo and 3.0-T gradient-echo T1-weighted imaging ($P > .05$). With the exception of minor susceptibility artifacts seen in acute and early subacute ICHs at 3.0-T T1-weighted gradient-echo imaging, no susceptibility artifacts were noticed. The ages of most lesions were identified correctly without significant differences between the two field strengths ($P > .05$), with the exception of the ages of acute ICHs, which were occasionally misinterpreted as early subacute lesions at 3.0 T.

CONCLUSION: At 3.0 T, all parts of acute and early subacute ICHs had significantly increased hypointensity on FLAIR and T2-weighted MR images as compared with the SIs of these lesions at 1.5 T. However, 1.5- and 3.0-T MR images were equivalent in the determination of acute to late subacute ICHs.

© RSNA, 2004

The numerous factors that contribute to the magnetic resonance (MR) imaging appearances of intracerebral hemorrhages (ICHs) and the complex signal intensity (SI) changes of these lesions have been extensively investigated in vitro and in vivo (1–9). Gomori et al (4,10–14) proposed explanations for the predominant MR SI patterns seen at a magnetic field strength of 1.5 T. Despite substantial variability in the regional and temporal SI patterns described in the literature (1,4,6,15–17), it is generally accepted that five stages of ICH (Table 1) can be distinguished according to their characteristic appearances at T1- and T2-weighted MR imaging (3,18–20).

It has been documented that at field strengths of 0.5–1.5 T, the most complex SI changes

TABLE 1
Evolution of ICHs at 1.5-T MR Imaging

| ICH Stage | Lesion Age | Affected Brain Compartment | Involved Magnetic Susceptible Substance | SI* | |
|------------|------------|----------------------------|---|----------------------|-----------------------|
| | | | | T1-weighted MR | T2-weighted MR |
| Hyperacute | <24 h | Intracellular | Oxyhemoglobin | Isointense | Slightly hyperintense |
| Acute | 1–3 d | Intracellular | Deoxyhemoglobin | Slightly hypointense | Hypointense |
| Subacute | | | | | |
| Early | >3 d | Intracellular | Methemoglobin | Very hyperintense | Hypointense |
| Late | >7 d | Extracellular | Methemoglobin | Very hyperintense | Very hyperintense |
| Chronic | >30 d | | | | |
| Center | | Extracellular | Hemachromes | Isointense | Slightly hyperintense |
| Rim | | Extracellular | Hemosiderin | Slightly hypointense | Very hypointense |

* SI of ICH compared with SI of normal brain parenchyma.

occur during the acute and subacute stages of ICH (4,6,21). At low and intermediate field strengths ranging from 0.02 to 0.5 T, several investigators (1,6,15–17) have described basically similar SI patterns in hemorrhages. It has been reported, however, that certain features of ICHs, such as a central area of hypointensity in acute lesions and a parenchymal rim of hypointensity on late to chronic lesions on T2-weighted MR images, can be demonstrated only at field strengths of 1.0 T or higher and have different appearances when they are imaged at field strengths of 0.5–0.6 T (central area of hypointensity) and 1.5 T (parenchymal rim of hypointensity) (4,21,22).

To our knowledge, only two case reports (23,24) have described MR imaging of subacute ICH at field strengths higher than 1.5 T. The investigators noticed that structures containing iron had an increased sensitivity to susceptibility effects coincidentally as a secondary finding at stroke imaging at a very high field strength of 8 T (23,24).

A new generation of whole-body MR imaging units with field strengths of 3.0 T is increasingly becoming available for routine imaging and is currently undergoing clinical evaluation. Therefore, the purpose of our study was to assess and describe the appearances of acute and subacute ICHs at 3.0-T high-field-strength MR imaging as compared with the appearances of these lesions at 1.5-T MR imaging.

MATERIALS AND METHODS

Patients

Our study was approved by the institutional review board, and written informed consent was obtained from the patients or their legal guardians.

From July 2002 to October 2002, 16 consecutive patients (age range, 6–77 years;

mean age, 42 years) with typical findings of parenchymal ICH that was diagnosed and staged by using clinical findings and computed tomography (CT) were examined. Ten patients were male (age range, 6–77 years; mean age, 41 years), and six were female (age range, 31–49 years; mean age, 43 years). No significant differences in mean age between the two groups ($P > .05$, Mann-Whitney U test) were observed. Because the appearance and development of hemorrhages also depend on the size and location of these lesions, only intraparenchymal lesions with a maximum diameter of 1.5–5.0 cm, as determined at CT, were evaluated; neither subarachnoid nor intraventricular lesions were studied. In total, 21 ICHs aged 24 hours to 1 month were included in this study. Three patients had two ICHs each, and one patient had three separate ICHs (Table 2).

The clinical age of ICH was based on the period between MR imaging examination and the start of bleeding, which was considered to be on the day of the onset of symptoms or on the day of the last relevant clinical event (eg, surgery). ICHs were classified as hyperacute (age, ≤ 24 hours), acute (age, between 24 hours and up to 3 days), early subacute (age, 3–7 days), late subacute (age, between 8 days and 1 month), or chronic (age, > 1 month) (3,18–20).

MR Imaging

Each patient underwent two MR imaging examinations (Gyrosan Intera; Philips Medical Systems, Best, the Netherlands)—one at a field strength of 1.5 T and the other at a field strength of 3.0 T—within 4 hours of each other. The initial field strength (1.5 or 3.0 T) was randomly selected. The imaging protocol consisted of T2-weighted fast spin-echo, fluid-attenuated inversion-recovery (FLAIR), and T1-weighted spin-echo and gradient-echo

TABLE 2
Summary of ICH Data

| Characteristic | No. of Patients ($n = 16$) | No. of Lesions ($n = 21$) |
|----------------|---------------------------------|--------------------------------|
| ICH cause | | |
| Spontaneous* | 6 | 8 |
| Trauma | 3 | 5 |
| Tumor | 4 | 4 |
| Infection | 3 | 4 |
| ICH age | | |
| <1 d | 0 | 0 |
| 1–3 d | 6 | 8 |
| >3–7 d | 5 | 7 |
| >7–31 d | 5 | 6 |
| >31 d | 0 | 0 |

* Includes hypertension-related, anticoagulant-related, and idiopathic lesions.

pulse sequences. Specific imaging parameters were as follows:

T2-weighted MR imaging.—T2-weighted fast spin-echo sequences were performed at 1.5 and 3.0 T identically by using 4000/90 (repetition time msec/echo time msec), a section thickness of 6 mm with an intersection gap of 1 mm, an echo train length of 15 echoes per echo train with an interecho time of 11.2 msec, and a matrix of 384×512 at a field of view of 250 mm. The water-fat shift was set to 1.25 pixels and kept constant at 1.5 and 3.0 T to ensure comparability of the susceptibility-induced effects (25); this setting resulted in bandwidths of 174 Hz per pixel at 1.5 T and 348 Hz per pixel at 3.0 T. The acquisition time (with two signals acquired) was 4 minutes 24 seconds at both field strengths.

FLAIR MR imaging.—FLAIR sequences were performed at 1.5 and 3.0 T identically by using 8000/120/2500 (repetition time msec/echo time msec/inversion time msec), a section thickness of 6 mm with an intersection gap of 1 mm, an echo train

length of 23 echoes per echo train with an interecho time of 10 msec, and a matrix of 192×256 at a field of view of 250 mm. The water-fat shift was set to 0.93 pixel and kept constant at 1.5 and 3.0 T; this setting resulted in bandwidths of 232 Hz per pixel at 1.5 T and 464 Hz per pixel at 3.0 T. The acquisition time (with two signals acquired) was 3 minutes 12 seconds at both field strengths.

T1-weighted MR imaging.—At 1.5 T, T1-weighted spin-echo sequences were performed with 580/15, a section thickness of 6 mm with an intersection gap of 1 mm, and a matrix of 384×512 at a field of view of 250 mm. The acquisition time (with two signals acquired) was 4 minutes 32 seconds.

At 3.0 T, owing to substantially prolonged T1 relaxation times, gradient-echo rather than spin-echo sequences were used for T1-weighted MR imaging to ensure adequate image contrast, which decreases with increasing field strength (26). To avoid potential susceptibility artifacts, the echo time was set to 2.3 msec, the lowest value possible. The other imaging parameters used were a 222-msec repetition time, an 80° flip angle, a 6-mm section thickness with a 1-mm intersection gap, a 384×512 matrix, and a 250-mm field of view. The acquisition time (with four signals acquired) was 2 minutes 57 seconds.

Image Analysis

Qualitative and quantitative analyses of SI score and contrast-to-noise ratio.—To determine the age of an ICH correctly, separate analyses of the core and the body of the lesion are required (21). The body of an ICH was defined as the bulk of the lesion volume central to the lesion margin, whereas the core of a lesion was defined as any central portion that contrasted with the lesion body on MR images (21).

Images of each ICH were presented in random order, with the imaging parameters masked, and evaluated in consensus by two board-certified radiologists (T.A., B.T.). Both radiologists had more than 10 years of experience in interpreting brain MR images and were blinded to the clinical and imaging data. For each pulse sequence performed at each field strength, the SIs of the core and body of the lesion were compared with the SI of the adjacent normal white matter, and a numerical value of -2 , -1 , 0 , $+1$, or $+2$ was assigned to indicate marked hypointensity, mild hypointensity, isointensity,

mild hyperintensity, or marked hyperintensity, respectively.

One observer (T.A.) quantitatively analyzed each ICH by using SI measurements in the core and body of the lesion that were obtained by using regions of interest drawn as large as possible. Regions of interest were placed at identical locations in each lesion at 1.5 and 3.0 T MR imaging. SI measurements were also performed in the adjacent normal white matter, which was used as the reference tissue. Background noise was measured in the phase-encoding direction with regions of interest drawn as large as possible. Each SI measurement was obtained three times by repeating measurements in adjacent sections. Contrast-to-noise ratios (CNRs) were calculated with signs to indicate a hyperintense (positive CNR) or hypointense (negative CNR) appearance, the determination of which is important for the correct staging of an ICH. However, for lesion detection, only the absolute values—not their signs—are important. The signed CNR of each lesion was calculated by using the following formula:

$$\frac{(\text{mean SI}_{\text{les}} - \text{mean SI}_{\text{ref}})}{\text{SD}_{\text{noise}}}$$

The absolute CNR of each lesion was calculated by using the following formula:

$$\frac{|\text{mean SI}_{\text{les}} - \text{mean SI}_{\text{ref}}|}{\text{SD}_{\text{noise}}}$$

In both equations, SI_{les} is the SI of the lesion; SI_{ref} , the SI of the reference tissue; and SD_{noise} , the standard deviation of the background noise.

Qualitative analysis of susceptibility-induced artifacts.—The two readers (T.A., B.T.) also judged the degree of apparent susceptibility artifacts in a lesion by assigning in consensus a numerical value of 0, meaning no artifacts; 1, meaning mild artifacts; or 2, meaning severe artifacts. Irregularly shaped hypointense streaks combined with SI inhomogeneity indicated the presence of mild susceptibility artifacts, whereas noticeable geometric distortion and even greater SI inhomogeneity within the core or body of a lesion indicated the presence of severe susceptibility artifacts.

Qualitative analysis of lesion age.—FLAIR, T2-weighted, and T1-weighted MR images of each lesion were presented simultaneously in random order of field strength with the imaging parameters masked. The readers (T.A., B.T.) had to determine in consensus the age of a lesion according to

its SI on T2- and T1-weighted images at field strengths of 1.5 and 3.0 separately. The stages of the ICHs were determined (Table 1), and numerical values for the different stages were assigned: 1 for hyperacute, 2 for acute, 3 for early subacute, 4 for late subacute, and 5 for chronic stage.

Qualitative image analysis, analysis of susceptibility-induced artifacts, and qualitative analysis of lesion age were performed at the same time. To avoid potential memory bias, quantitative image analysis was performed 3 months later.

Statistical Analyses

During the design of the study, a power analysis was performed by using preliminary SI measurements obtained in three test patients with acute ICH who were not included in the final study population. For the central parts of the ICHs, the mean SI differences between field strengths of 1.5 and 3.0 T at FLAIR and T2-weighted MR imaging were more than twofold greater than their standard deviations. Therefore, a minimum of five lesions were considered appropriate for an intended power of 0.8 or greater ($P \leq .05$) at subsequent power analysis.

Statistical analyses of SI scores, susceptibility artifacts, and lesion age were performed by using the χ^2 test to determine statistically significant differences between 1.5- and 3.0-T MR imaging. Lesion CNRs were analyzed by using the Wilcoxon signed-rank test (27). A P value of less than or equal to .05 was considered to indicate statistical significance. The software used to perform the statistical analyses was SPSS, version 11.0 (SPSS, Chicago, Ill). Power analysis was performed by using in-house software (medweb.uni-muenster.de/institute/imib/lehre/skripte/biomasche/bio/fallz.html, Institut für Medizinische Informatik und Biomathematik, University of Muenster, Muenster, Germany).

RESULTS

Qualitative and Quantitative Analyses of SI Scores and CNRs

CNRs of the bodies and cores of ICHs at each stage and at both field strengths, as qualitatively calculated by the two readers, are listed in Table 3, and the corresponding SI scores are illustrated in Figure 1. Separate analyses for the bodies and cores of lesions were performed with all sequences. Figures 2 and 3 are image examples.

At 3.0-T T2-weighted MR imaging, signed CNRs and SI scores for all parts of

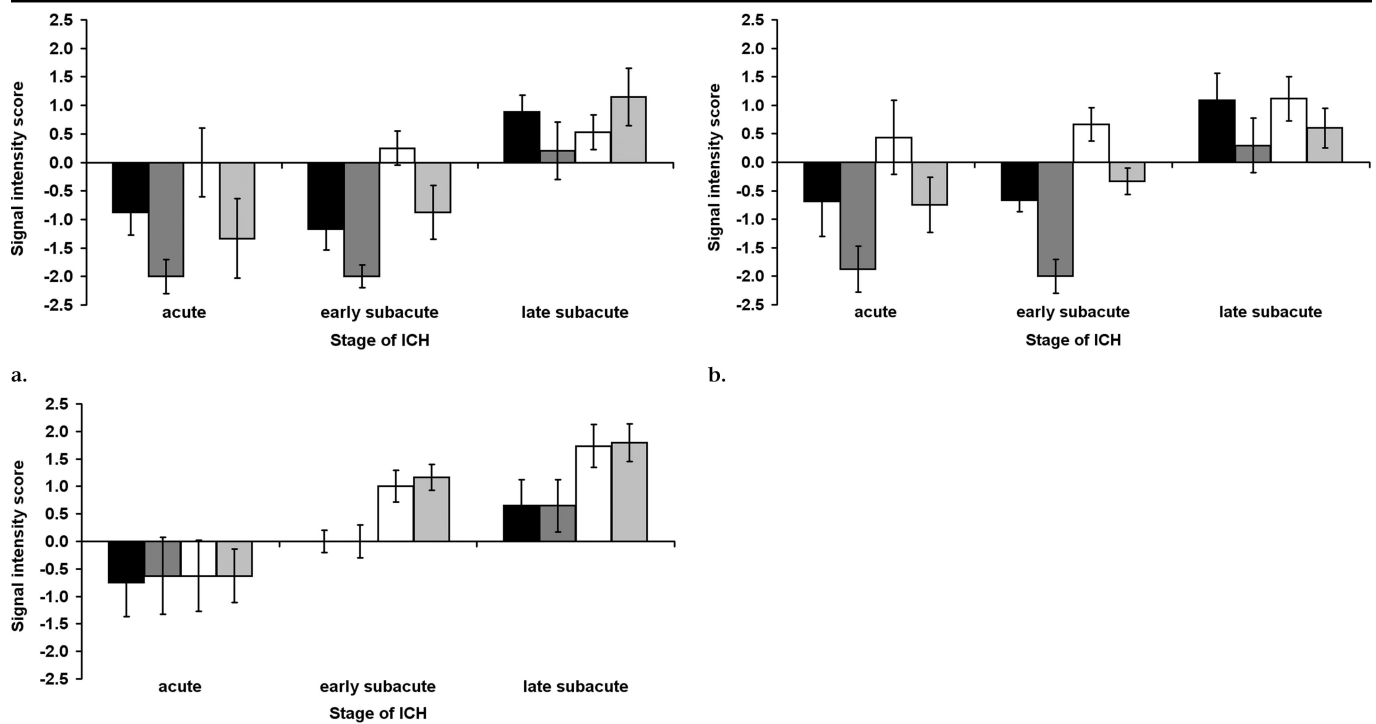


Figure 1. Mean SI scores (and standard deviations [vertical lines]) for ICH cores at 1.5 T (black bars), ICH cores at 3.0 T (dark gray bars), ICH bodies at 1.5 T (white bars), and ICH bodies at 3.0 T (light gray bars) determined at (a) T2-weighted, (b) FLAIR, and (c) T1-weighted MR imaging.

the ICHs at all stages—except the bodies of lesions imaged during the late subacute stage, which had increased signed CNRs and SI scores at 3.0 T—were lower than the corresponding values at 1.5-T T2-weighted MR imaging (Table 3; Fig 1a; Fig 2, A, B; Fig 3, A, B). Maximum absolute CNRs for all parts of the ICHs at all stages—except the bodies of lesions imaged during the late subacute stage, which showed a maximum absolute CNR at 1.5 T—were measured at 3.0-T MR imaging.

Significant differences in signed CNR, absolute CNR, and SI score between 1.5- and 3.0-T MR imaging were observed in all parts of the ICHs during the early subacute stage and in the lesion cores during the acute stage ($P \leq .05$). Maximum differences in signed and absolute CNRs between 1.5- and 3.0-T MR imaging were observed in ICH cores during the acute stage. The bodies of acute and early subacute ICHs were hypointense on 3.0-T T2-weighted MR images, differing significantly from the ICH bodies seen on 1.5-T T2-weighted MR images, which were isointense to hyperintense during this stage ($P \leq .05$) (Fig 1a).

With use of the FLAIR sequences at the higher field strength of 3.0 T, all parts of

TABLE 3
Signed CNRs of the Cores and Bodies of ICHs at Different Stages and Field Strengths

| ICH Region and MR Field Strength | Acute Stage | Early Subacute Stage | Late Subacute Stage |
|----------------------------------|-----------------|----------------------|---------------------|
| T2-weighted MR | | | |
| Core | | | |
| 1.5 T | -8.5 ± 5.9 | -9.9 ± 5.3 | 10.9 ± 3.6 |
| 3.0 T | -30.6 ± 5.1 | -25.2 ± 5.3 | 7.6 ± 3.2 |
| Body | | | |
| 1.5 T | 1.3 ± 5.7 | 3.6 ± 2.5 | 11.9 ± 5.2 |
| 3.0 T | -9.1 ± 7.2 | -7.5 ± 4.3 | 17.2 ± 7.6 |
| FLAIR MR | | | |
| Core | | | |
| 1.5 T | -4.7 ± 2.1 | -5.3 ± 3.2 | 12.8 ± 3.8 |
| 3.0 T | -11.0 ± 3.6 | -10.7 ± 2.8 | 4.5 ± 7.0 |
| Body | | | |
| 1.5 T | 2.3 ± 1.9 | 5.2 ± 3.3 | 14.9 ± 3.2 |
| 3.0 T | -7.3 ± 4.1 | -5.5 ± 3.3 | 8.4 ± 7.4 |
| T1-weighted MR | | | |
| Core | | | |
| 1.5 T | -5.0 ± 5.7 | 0.4 ± 2.0 | 10.7 ± 7.2 |
| 3.0 T | -6.7 ± 7.9 | 0.1 ± 2.3 | 13.5 ± 8.2 |
| Body | | | |
| 1.5 T | -3.7 ± 5.7 | 7.1 ± 5.3 | 15.7 ± 3.9 |
| 3.0 T | -5.1 ± 8.4 | 12.6 ± 6.2 | 20.0 ± 10.7 |

Note.—Data are mean CNRs \pm standard deviations.

the depicted ICHs at all stages had lower signed CNRs and SI scores compared with

their CNRs and SI scores at 1.5 T (Table 3; Fig 1b; Fig 2, C, D; Fig 3, C, D). Maximum

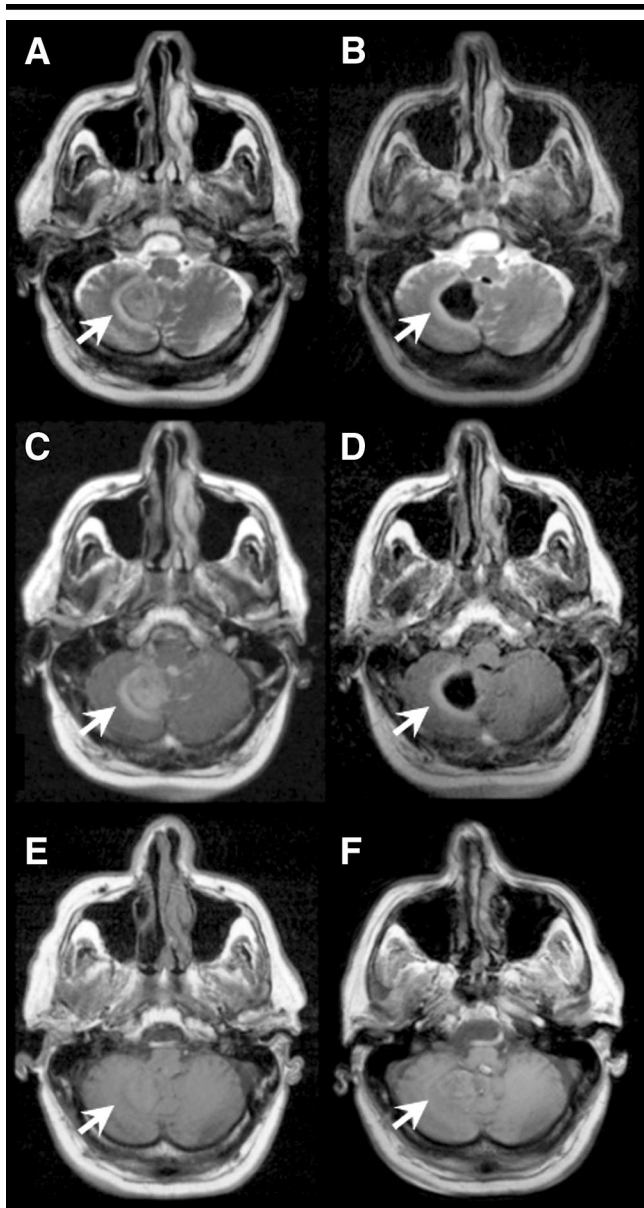


Figure 2. Acute ICH (arrow) in 77-year-old man who received anticoagulative medication and underwent MR imaging on the 2nd day after the onset of clinical symptoms (dizziness and nausea). Transverse T2-weighted (4000/90) (A and B), FLAIR (8000/120/2500) (C and D), and T1-weighted (580/15 at 1.5 T, 222/2.3 at 3.0 T) (E and F) MR images obtained at 1.5 T (A, C, and E) and 3.0 T (B, D, and F). A–D, On T2-weighted and FLAIR images, the ICH (arrow) is isointense to hyperintense at 1.5 T (A and C) but markedly hypointense at 3.0 T (B and D).

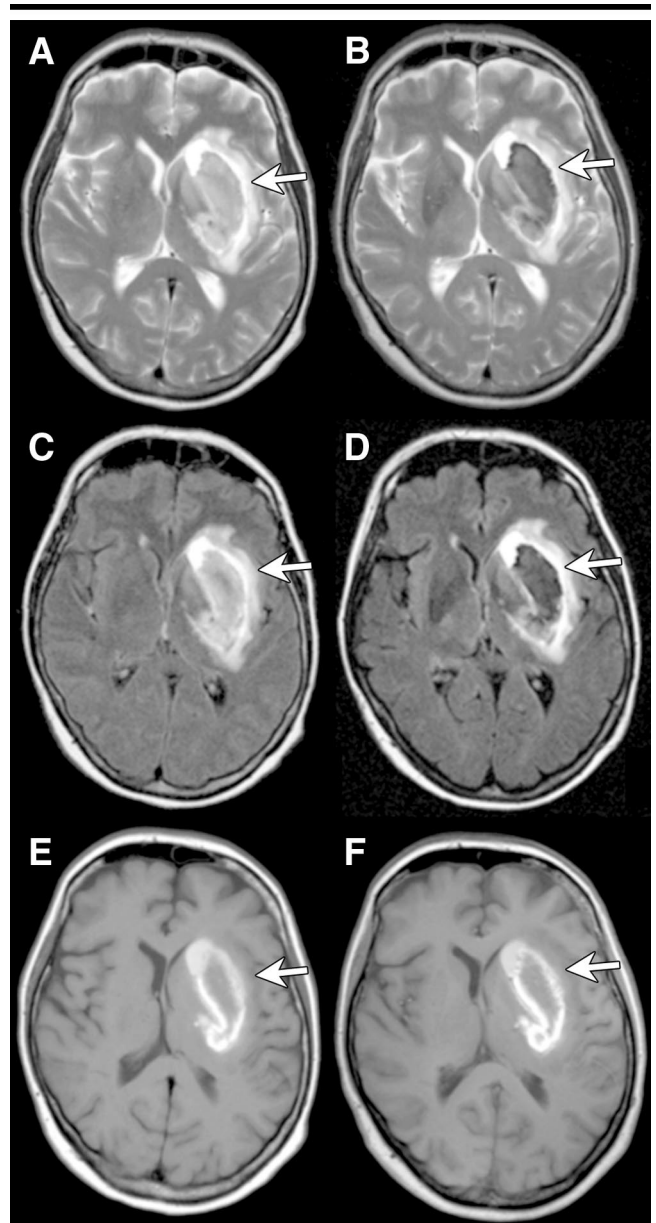


Figure 3. Early subacute ICH (arrow) in 56-year-old woman with arterial hypertension who underwent MR imaging on the 6th day after the onset of clinical symptoms (right-sided hemiplegia). Transverse T2-weighted (4000/90) (A and B), FLAIR (8000/120/2500) (C and D), and T1-weighted (580/15 at 1.5 T, 222/2.3 at 3.0 T) (E and F) MR images obtained at 1.5 T (A, C, and E) and 3.0 T (B, D, and F). A–D, On T2-weighted and FLAIR images, the ICH (arrow) is hyperintense at 1.5 T (A and C) but hypointense at 3.0 T (B and D).

absolute CNRs were measured for the bodies and cores of acute ICHs and for the cores of early subacute lesions at 3.0 T, whereas the bodies of early subacute lesions and all parts of late subacute lesions showed maximum absolute CNRs at 1.5 T. Significant ($P \leq .05$) differences in signed CNR, absolute CNR, and SI score between the two field strengths

were observed for all parts of acute and early subacute ICHs. Differences in maximum signed CNR and absolute CNR between 1.5- and 3.0-T MR imaging were observed in the bodies of early subacute lesions. The bodies of acute and early subacute ICHs were hypointense on 3.0-T FLAIR MR images, differing significantly from the ICH bodies depicted on

1.5-T FLAIR MR images, which were hyperintense during this stage ($P \leq .05$) (Fig 1b).

At T1-weighted MR imaging, no significant differences in signed CNR, absolute CNR, or SI score ($P > .05$) at any investigated stage of ICH—whether the core or the body of the lesion—were observed between spin-echo images acquired at 1.5 T and gradient-echo images acquired

at 3.0 T (Table 3; Fig 1c; Fig 2, E, F; Fig 3, E, F).

Qualitative Analysis of Susceptibility-induced Artifacts

Neither FLAIR and T2-weighted fast spin-echo MR sequences performed at 1.5 and 3.0 T nor T1-weighted spin-echo sequences performed at 1.5 T yielded noticeable susceptibility artifacts. T1-weighted gradient-echo MR images obtained at 3.0 T showed minor susceptibility artifacts in acute and early subacute ICHs (mean score \pm standard deviation: 0.8 ± 0.4 during acute stage, 0.3 ± 0.5 during early subacute stage) (Fig 4).

Qualitative Analysis of ICH Age

The ages of most of the ICHs were correctly determined at 1.5- and 3.0-T MR imaging (Table 4), without significant differences ($P > .05$) between the two field strengths. However, one acute lesion was classified as early subacute at 1.5 T. In addition, three acute and two late subacute lesions were misinterpreted as early subacute at 3.0 T.

DISCUSSION

Acute and subacute ICHs undergo rapid and complex SI changes, which are influenced by intrinsic, biologic, and extrinsic factors (18). The contributing intrinsic and biologic factors include the time from the onset of ICH; the source, size, and location of the lesion; the effects of paramagnetic forms of hemoglobin; the clot matrix formation; the red blood cell concentration; the PO_2 ; the arterial versus venous origin of the lesion; the tissue pH; the intracellular protein concentration; the presence or absence of a blood-brain barrier; and the patient's overall health. Extrinsic factors that affect the appearance of ICH include the pulse sequence type, the sequence parameters, the receiver bandwidth, and the applied magnetic field strength (18).

When MR imaging systems with operating field strengths of 1.0–1.5 T—previously referred to as high-field-strength units—were introduced, the intrinsic and extrinsic factors that contribute to SI changes of ICH were extensively investigated in vitro and in vivo (1,2,4–9). It was shown that especially the central area of hypointensity in ICHs, which has been described as the most critical factor in the detection of these lesions (22), was depicted only at field strengths higher than 1.0 T. As proved in vitro, this ap-

pearance increases quadratically with magnetic field strength (4,19).

Whole-body MR imaging units with field strengths of 3.0 T have recently become available for routine imaging and are currently undergoing clinical evaluation. Because the appearance of ICH is influenced by several mechanisms that mainly depend on the magnetic field strength, the investigation of ICH at 3.0 T may help to improve knowledge about the MR imaging appearance of this lesion and to clarify the potential further mechanisms that lead to altered SI.

At 1.5 T, our CNR calculations and reader observations of SI were associated with the same patterns on T2- and T1-weighted MR images of acute, early, and late subacute ICHs, as initially described by Gomori et al (4), and are in excellent accordance with the findings in previous studies (3,18).

At 3.0 T, the cores and bodies of acute and early subacute ICHs were markedly hypointense on FLAIR and T2-weighted MR images. The hypointensity of early subacute ICH bodies decreased but re-

mained at 3.0 T, differing significantly from the bodies of lesions imaged at 1.5 T, which were hyperintense during this stage on FLAIR and T2-weighted MR images.

In contrast to the findings described in previous reports comparing 0.6- and 1.5-T field strengths (22), the hypointense areas seen on FLAIR and T2-weighted MR images of acute and early subacute ICH cores in the current study persisted similarly at the two field strengths, and the mean negative CNR and mean SI score observed at 1.5 T were improved at 3.0 T. However, the mean positive CNR and mean SI score for late subacute ICHs were lower compared with these values at 1.5 T.

The hypointense areas seen on T2-weighted MR images during the acute and early subacute stages are caused by phase coherency loss of water molecules diffusing in and out of intact red blood cells that contain magnetic susceptible substances such as deoxyhemoglobin or methemoglobin (3,14,20). Because susceptibility effects depend on field strength, at 3.0 T, apparently minimal amounts of intracellular de-

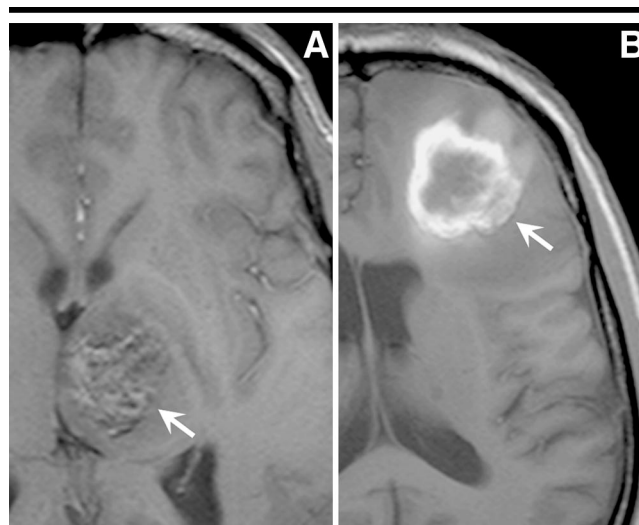


Figure 4. Transverse T1-weighted gradient-echo MR images (222/2.3) obtained at 3.0 T show apparent susceptibility artifacts (irregularly shaped hypointense streaks combined with SI inhomogeneity) in A, acute, and B, early subacute ICHs (arrow).

TABLE 4
Qualitative Analysis of Lesion Stages at MR Imaging

| ICH Stage | No. of Lesions | Correct Stage at 1.5 T MR | Correct Stage at 3.0 T MR |
|----------------|----------------|---------------------------|---------------------------|
| Acute | 8 | 7 | 5 |
| Early subacute | 7 | 8 | 12 |
| Late subacute | 6 | 6 | 4 |

Note.—Data are numbers of ICH lesions.

oxyhemoglobin or methemoglobin are required to evoke these effects and cause hypointensity or even reduce SI.

Increased positive CNRs and SI scores for the bodies of early and late subacute ICHs at 1.5 T are caused by beginning red cell lysis, which starts peripherally owing to intrinsic tissue factors (28) and higher oxygen levels, which are required for the oxidization of deoxyhemoglobin to methemoglobin (3). As lysis occurs, the T2 shortening that has resulted from the compartmentalization of methemoglobin is lost. In addition, the high water content of the lysed red blood cells leads to an increase in proton density and in SI at the hemorrhage periphery on T2-weighted MR images.

At 3.0 T, obviously greater amounts of extracellular methemoglobin and higher water contents are required to prevent susceptibility-induced effects and to alter the CNR and the SI score for the periphery of an early subacute ICH so as to result in hyperintensity on FLAIR and T2-weighted MR images. In the current study, however, the mean CNR and the mean SI score for the bodies of late subacute lesions indicated disparate changes. At 3.0-T MR imaging, the mean CNR and the mean SI score were higher on T2-weighted images but lower on FLAIR images as compared with these values at 1.5-T MR imaging. Such findings are probably caused by the increased content of free water that is undergoing fluid attenuation (18,29).

The different appearances of acute and early subacute parenchymal ICHs at 1.5- and 3.0-T MR imaging were also reflected in the results of the qualitative analysis of lesion age. The acute ICHs that were correctly graded at 1.5 T were more often judged to be "acute or early subacute" at 3.0 T because of their markedly hypointense appearance at higher field strengths. However, these differences were not significant ($P > .05$) in our patient population. Because determination of the age of early subacute ICHs requires both T1- and T2-weighted MR imaging, no significant difference ($P > .05$) between the two field strengths was observed in the staging of these lesions. The hyperintense body of early subacute lesions on T1-weighted MR images in combination with an isointense to hypointense core always pointed toward the correct diagnosis of early subacute ICH at either field strength. Despite this, it was sometimes striking to the observers when an early subacute lesion with a hyperintense periphery on T1-weighted MR images was markedly hypointense in all areas on T2-weighted MR images.

Despite the different techniques used to

perform T1-weighted MR imaging (ie, 1.5-T spin echo and 3.0-T gradient echo), no significant differences were observed between 1.5- and 3.0-T T1-weighted imaging. The mean CNR and mean SI score at 3.0 T did not change significantly in comparison to those observed at 1.5 T. Therefore, field strength did not affect the rate or degree of development of hyperintensity on T1-weighted MR images. These results correspond to findings observed in previous studies (21,22). Because the paramagnetic T1 shortening caused by methemoglobin is supposed to inversely vary with field strength, the formation of methemoglobin is expected to be better demonstrated at 1.5 T (21). Despite this, an increased signal-to-noise ratio at 3.0 T may explain the lack of differences in the depiction of methemoglobin between 1.5- and 3.0-T MR imaging.

Our study had several limitations. The pathologic verification of ICH was incomplete. Tumor-induced ICH was confirmed pathologically in only two of four patients. However, a strong history of neurologic deterioration after either trauma or anticoagulant therapy and the presence of characteristic CT findings enabled confident diagnoses of ICH.

No hyperacute ICHs (aged a few minutes up to a few hours) were evaluated because, to ensure that conditions were sufficient to compare ICHs at either field strength, the time interval between the 1.5- and 3.0-T examinations could not be shortened. Because the most complex SI changes occur during the acute and subacute stages of ICH at field strengths of 0.5–1.5 T (4,6,21), no chronic parenchymal ICHs were included in our study. However, considering our results and those of previous studies, it would have been revealing to also investigate the specific appearance of hemosiderin deposits in this lesion type. Seidenwurm et al (21) noticed significant differences in the appearances of chronic ICHs at 0.5- and 1.5-T MR imaging. Therefore, the depiction of even further increased and probably prolonged hypointensity of chronic ICHs at 3.0 T would be expected.

Furthermore, no serial investigations were performed at different field strengths in this study because most of the patients with acute or subacute ICH were seriously ill and often required intensive care. Therefore, the acute, early subacute, and late subacute ICH groups consisted of more or less heterogeneous populations of lesions that differed in size, location, origin (arterial vs venous), and cause. These differences reduce the comparability of observed SIs between differ-

ent ICH stages and impair the exact assessment of lesion progression during the course of time. The question of whether there would have been significant differences in the determination of the ages of acute and early subacute lesions between the two field strengths in a larger patient population also remains.

It has been reported that gradient-echo and spin-echo MR imaging sequences have higher sensitivity to susceptibility-induced effects, which are required to detect and correctly stage ICH, than do fast spin-echo sequences (21,30,31), and it remains unclear whether the use of these sequences would have revealed even greater differences between the two field strengths. Despite this, fast spin echo is currently the sequence of choice for routine clinical imaging. Furthermore, our study was not focused on the sensitivity of the detection of small degrees of parenchymal ICH, but rather it was focused solely on the CNR and SI characteristics of ICHs seen at 1.5- and 3.0-T MR imaging in the clinical setting. Therefore, only fast spin-echo—and no gradient-echo or spin-echo sequences—were used for T2-weighted imaging.

Finally, the quantitative and qualitative analyses were performed by the same observer (T.A.) and thus were possibly impaired by memory bias in terms of remembered ratings, which could not be excluded with absolute certainty. However, the qualitative analysis was performed 3 months after the quantitative analysis (by T.A. and B.T.). We believed that this time interval was long enough to reduce the potential memory bias to a negligible level.

In summary, despite the fact that all parts of the depicted acute and early subacute ICHs had significantly increased hypointensity on 3.0-T FLAIR and T2-weighted MR images, the images obtained at 1.5 and 3.0 T were equivalent in the determination of the ages of acute to late subacute ICHs. According to our findings, knowledge of the image characteristics of ICHs at 1.5 and 3.0 T is required to compare and correctly appreciate the progression of these lesions.

References

1. Sipponen JT, Sepponen RE, Sivula A. Nuclear magnetic resonance (NMR) imaging of intracerebral hemorrhage in the acute and resolving phases. *J Comput Assist Tomogr* 1983; 7:954–959.
2. Bradley WG Jr, Schmidt PG. Effect of methemoglobin formation on the MR appearance of subarachnoid hemorrhage. *Radiology* 1985; 156:99–103.
3. Bradley WG Jr. MR appearance of hemor-

- rhage in the brain. *Radiology* 1993; 189: 15–26.
4. Gomori JM, Grossman RI, Goldberg HI, Zimmerman RA, Bilaniuk LT. Intracranial hematomas: imaging by high-field MR. *Radiology* 1985; 157:87–93.
 5. Di Chiro G, Brooks RA, Girton ME, et al. Sequential MR studies of intracerebral hematomas in monkeys. *AJNR Am J Neuroradiol* 1986; 7:193–199.
 6. Zimmerman RD, Heier LA, Snow RB, et al. Acute intracranial hemorrhage: intensity changes on sequential MR scans at 0.5 T. *AJR Am J Roentgenol* 1988; 150:651–661.
 7. Hayman LA, McArdle CB, Taber KH, et al. MR imaging of hyperacute intracranial hemorrhage in the cat. *AJNR Am J Neuroradiol* 1989; 10:681–686.
 8. Brooks RA, Di Chiro G, Patronas N. MR imaging of cerebral hematomas at different field strengths: theory and applications. *J Comput Assist Tomogr* 1989; 13: 194–206.
 9. Clark RA, Watanabe AT, Bradley WG Jr, Roberts JD. Acute hematomas: effects of deoxygenation, hematocrit, and fibrin-clot formation and retraction on T2 shortening. *Radiology* 1990; 175:201–206.
 10. Gomori JM, Grossman RI, Goldberg HI, et al. High-field spin-echo MR imaging of superficial and subependymal siderosis secondary to neonatal intraventricular hemorrhage. *Neuroradiology* 1987; 29:339–342.
 11. Gomori JM, Grossman RI, Yu-IP C, Asakura T. NMR relaxation times of blood: dependence on field strength, oxidation state, and cell integrity. *J Comput Assist Tomogr* 1987; 11:684–690.
 12. Gomori JM, Grossman RI, Hackney DB, et al. Variable appearances of subacute intracranial hematomas on high-field spin-echo MR. *AJR Am J Roentgenol* 1988; 150:171–178.
 13. Gomori JM, Grossman RI, Steiner I. High-field magnetic resonance imaging of intracranial hematomas. *Isr J Med Sci* 1988; 24:218–223.
 14. Gomori JM, Grossman RI. Mechanisms responsible for the MR appearance and evolution of intracranial hemorrhage. *Radiographics* 1988; 8:427–440.
 15. Bydder GM, Pennock JM, Porteous R, et al. MRI of intracerebral haematoma at low field (0.15T) by using T2 dependent partial saturation sequences. *Neuroradiology* 1988; 30:367–371.
 16. Edelman RR, Johnson K, Buxton R, et al. MR of hemorrhage: a new approach. *AJNR Am J Neuroradiol* 1986; 7:751–756.
 17. Sipponen JT, Sepponen RE, Tanttu JJ, Sivula A. Intracranial hematomas studied by MR imaging at 0.17 and 0.02 T. *J Comput Assist Tomogr* 1985; 9:698–704.
 18. Parizel PM, Makkat S, Van Miert E, et al. Intracranial hemorrhage: principles of CT and MRI interpretation. *Eur Radiol* 2001; 11:1770–1783.
 19. Thulborn KR, Brady TJ. Iron in magnetic resonance imaging of cerebral hemorrhage. *Magn Reson Q* 1989; 5:23–38.
 20. Hayman LA, Taber KH, Ford JJ, Bryan RN. Mechanisms of MR signal alteration by acute intracerebral blood: old concepts and new theories. *AJNR Am J Neuroradiol* 1991; 12:899–907.
 21. Seidenwurm D, Meng TK, Kowalski H, Weinreb JC, Kricheff II. Intracranial hemorrhagic lesions: evaluation with spin-echo and gradient-refocused MR imaging at 0.5 and 1.5 T. *Radiology* 1989; 172: 189–194.
 22. Weingarten K, Zimmerman RD, Deo-Narine V, et al. MR imaging of acute intracranial hemorrhage: findings on sequential spin-echo and gradient-echo images in a dog model. *AJNR Am J Neuroradiol* 1991; 12:457–467.
 23. Novak V, Kangarlu A, Abduljalil A, et al. Ultra high field MRI at 8 Tesla of subacute hemorrhagic stroke. *J Comput Assist Tomogr* 2001; 25:431–435.
 24. Chakeres DW, Abduljalil AM, Novak P, Novak V. Comparison of 1.5 and 8 Tesla high-resolution magnetic resonance imaging of lacunar infarcts. *J Comput Assist Tomogr* 2002; 26:628–632.
 25. Oehler MC, Schmalbrock P, Chakeres D, Kurucay S. Magnetic susceptibility artifacts on high-resolution MR of the temporal bone. *AJNR Am J Neuroradiol* 1995; 16:1135–1143.
 26. Bottomley PA, Foster TH, Argersinger RE, Pfeifer LM. A review of normal tissue hydrogen NMR relaxation times and relaxation mechanisms from 1–100 MHz: dependence on tissue type, NMR frequency, temperature, species, excision, and age. *Med Phys* 1984; 11:425–448.
 27. Armitage P, Berry G. *Statistical methods in medical research*. 2nd ed. Oxford, England: Blackwell, 1987.
 28. Taber KH, Migliore PJ, Pagani JJ, et al. Temporal changes in the oxidation state in *in vitro* blood. *Invest Radiol* 1990; 25: 240–244.
 29. Hackney DB, Atlas SW, Grossman RI, et al. Subacute intracranial hemorrhage: contribution of spin density to appearance on spin-echo MR images. *Radiology* 1987; 165:199–202.
 30. Reimer P, Allkemper T, Schuierer G, Peters PE. Brain imaging: reduced sensitivity of RARE-derived techniques to susceptibility effects. *J Comput Assist Tomogr* 1996; 20:201–205.
 31. Allkemper T, Reimer P, Schuierer G, Peters PE. Study of susceptibility-induced artefacts in GRASE with different echo train length. *Eur Radiol* 1998; 8:834–838.